Hindawi
Geofluids
Volume 2021, Article ID 3356645, 8 pages
https://doi.org/10.1155/2021/3356645

Research Article

Multiscale Research on Pore Structure Characteristics and Permeability Prediction of Sandstone

M. A. Shi-Jia,[1,2] L. I. N. Yuan-Jian,[1,3] L. I. U. Jiang-Feng,[1,2] Kundwa Marie Judith,[1] Ishimwe Hubert,[4] and W. A. N. G. Pei-lin[1]

[1]*The State Key Laboratory for GeoMechanics and Deep Underground Engineering, and School of Mechanics and Civil Engineering, China University of Mining and Technology, Xuzhou 221000, China*
[2]*Key Laboratory of Deep Earth Science and Engineering (Sichuan University), Ministry of Education, Chengdu, China*
[3]*School of Education, Nanchang Institute of Science and Technology, Nanchang 330108, China*
[4]*School of Resources and Geosciences, China University of Mining and Technology, Xuzhou 221116, China*

Correspondence should be addressed to L. I. N. Yuan-Jian; yuanjianlin@cumt.edu.cn and L. I. U. Jiang-Feng; jeafliu@hotmail.com

Received 20 September 2021; Accepted 3 November 2021; Published 30 November 2021

Academic Editor: Afshin Davarpanah

The random existence of many irregular pore structures in geotechnical materials has a decisive influence on its permeability and other macroscopic properties. The analysis and characterization of the micropore structure of the material and its permeability are of great significance for geotechnical engineering. In this study, digital images with different magnifications were used to examine the pore structure and permeability of sandstone samples. The image processing method is used to obtain binary images, and then, the pore size distribution method is used to calculate the pore size distribution. Therefore, based on the Hagen-Poiseuille formula, we get the prediction value of material's permeability and compare it with the value obtained from mercury intrusion porosimetry (MIP). It is found that different microscopic images with different magnification and various statistical methods of pore size have a specific influence on the characterization of pore structure and permeability prediction. The porosity of different magnifications is not the same, and the results obtained at higher magnifications are more consistent with the results obtained with MIP. With the increase of magnification, we can observe more pores in large sizes. The effect of CPSD (continuous pore size distribution) in pore size statistics is better than that of DPSD (discrete pore size distribution). In permeability prediction, the prediction result of higher magnification images are closer to the instrument test value, and the value of DPSD is more significant than that of CPSD. In future research, an appropriate method should be selected to obtain a reasonable prediction of the permeability of the target material.

1. Introduction

For the characterization of sandstone reservoirs, porosity, pore size distribution, and permeability are essential parameters for reservoir evaluation. A sandstone sample usually contains many irregular, variable-sized, randomly distributed, interconnected pores, which become the main accumulation places and percolation channels for hydrocarbon fluids. The porosity determines the storage capacity of hydrocarbons, while the pore size distribution and permeability directly affect the transport capacity of hydrocarbons [1–4]. Therefore, the macroscopic gas permeability experiment can usually obtain the gas transport mode but cannot reveal its transport mechanism [5–8]. On the other hand, microscopic analysis can observe the development of pores and fractures in the sample, which provides a direct basis for studying the seepage evolution mechanism of a rock mass. Therefore, microscopic analysis of the pore structure and permeability can help to reveal the distribution of oil and gas in sandstone reservoirs and the microscopic transport mechanism [9, 10].

The main methods of studying microscopic pore structure in the existing work are divided into two categories. The first category methods use the physical measure to evaluate the pore throat radius distribution, connectivity, and pore structure parameters, and it includes MIP, nitrogen

adsorption, and nuclear magnetic resonance (NMR) [8, 11, 12]. The second category methods use precision instruments to obtain digital images containing the microscopic morphology of a sample, such as computed tomography (CT), scanning electron microscope (SEM), and transmission electron microscopy (TEM) [13, 14]. The first category methods are widely used in existing research. Still, it has some disadvantages: the pore size distribution of the specimen can be well characterized by MIP, but the higher pressure can affect the pore structure of the sample itself, thus affecting the characterization of the pore structure. Nitrogen adsorption can only characterize pores with a radius of less than 100 nm. NMR is a nondestructive technique that simulates the specimen and indicates a wide pore size, but its accuracy depends on calibration experiments. These pore structure characterization methods all have a common disadvantage. They do not allow visual observation of the pore structure of the rock samples [1, 15].

For the second category, such as CT, SEM, and TEM, the pore structure of the sample can be directly observed. The three-dimensional pore structure of the sample can be seen using computed tomography, but it is difficult to characterize the pores on the nanoscale. TEM is suitable for measuring sample's morphology, but the test requires a relatively thin piece to allow the passage of electrons. SEM can characterize the pores at different scales, from the nanoscale to the millimeter scale. Furthermore, the previous study found specific differences in the pore structure properties (porosity, pore size distribution, etc.) characterized by SEM images of different scales [2, 3, 13]. Therefore, different magnifications of SEM images were performed in this study to examine and quantify the pore structure of the same sample.

The next section of this paper is organized as a follow-up: the SEM images are first acquired at different magnifications and studied from different scales. Then, a reasonable threshold value is selected based on the correlation threshold determination algorithm to binarise the image segmentation. The pore size distribution is then calculated based on the discrete and continuous pore size distribution algorithms. Finally, permeability prediction is based on the Hagen-Poiseuille equation and the previous pore size distribution information. Simultaneously, the results of the digital image-based calculations are compared to those of laboratory experiments (e.g., mercury pressure experiments and gas permeability experiments) to verify the adaptability and accuracy of the relevant algorithms.

2. Materials and Methodology

2.1. SEM Image Scanning and Image Information. Using a Quantatm 250 scanning electron microscope introduced by China University of Mining and Technology from the FEI Company in the United States, sandstone is scanned by SEM. The equipment has an excellent stable operation of ultralow vacuum/low vacuum and sample signal collection effect. The density of the intact sandstone sample is 2.565 $\pm 0.1\,\mathrm{g/cm^2}$. The porosity measured by the mercury injection method is 4.52%. The main mineral components of sandstone include quartz, potassium feldspar, plagioclase, calcite, siderite, and clay minerals (Illite, Kaolinite, Chlorite, and Smectite). The collected sandstone samples are 10 mm $*$ 10 mm $*$ 10 mm fragments (as shown in Figure 1). SEM images of sandstone with different magnifications are obtained by a scanning electron microscope, with 600-fold, 1200-fold, and 2000-fold, respectively. The resolution of the SEM image is relatively high, and it is easier to obtain digital images of different scales. While CT can get pore sizes on the nanoscale, SEM can acquire pores as tiny as a micron. The pixel accuracy of different images is shown in Table 1. As can be observed that the increase of magnification, the smaller the pixel accuracy of the image is, that is, the smaller the pore structure is observed.

2.2. Methodology

2.2.1. Method for Calculating Porosity. Following binary segmentation of the digital image, pores' pixels are assigned a value of 0, while the remaining matrix is assigned a value of 1. The porosity φ is calculated as follows:

$$\varphi = \frac{S_\varphi}{S} \times 100\%, \tag{1}$$

where φ stands for porosity, %; S_φ represents the area of the pore; S represents the total area of the image.

2.2.2. Characterization of Pore Size Distribution. There are two main algorithms for determining the pore size distribution (PSD) of a sample using digital images: DPSD and CPSD. The main difference between DPSD and CPSD is that CPSD takes into account pore geometry when extracting pore size distribution. The principal idea of the "continuous PSD" at a specific pore radius r_s is to determine the amount of pore volume (3D) or a rather pore area (2D), which potentially can be covered with spheres and circles of the radius r_s in 3D and 2D, respectively. Even a single unconnected pore object becomes not a single value only but instead possesses its PSD, as it is inspected individually. In contrast, the principle of the CPSD algorithm is similar to the mercury injection method. For DPSD, the sizes of their volume and their area are determined subsequently for the 3D case and the 2D case, respectively. A respective pore radius may be determined for each pore object from such volume or area by calculating the radius of its size-equivalent sphere or circle. The primary approach is to convert irregular pores to circles or spheres using the equal area principle [16]. To further understand the binary principle, two images are presented in Figure 2.

2.2.3. Permeability Calculation. Hagen-Poiseuille law is a physical law in nonideal fluid dynamics. It proposes that when an incompressible Newtonian fluid passes through a long cylindrical tube with a particular section in laminar flow [8, 17], the velocity distribution of the section is

$$v = \frac{\Delta P}{4\mu L}\left(R^2 - r^2\right), \tag{2}$$

where r is the distance from the center of the circle; ΔP is the

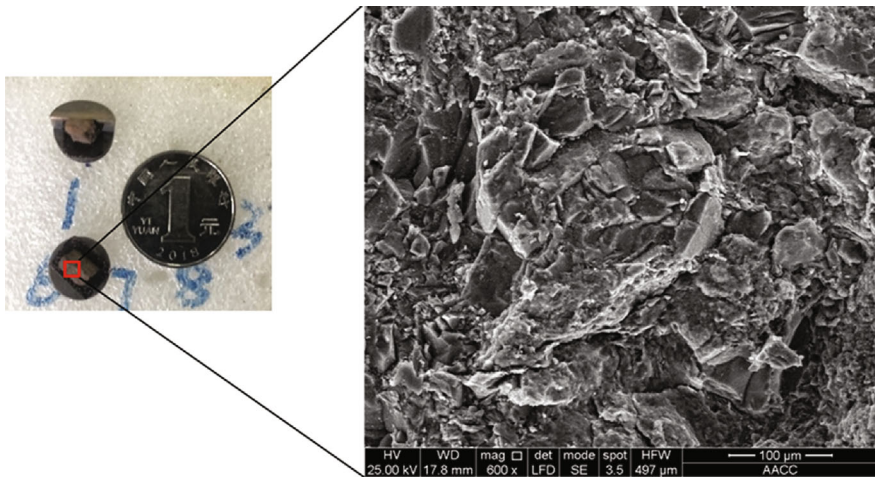

Figure 1: A sandstone sample and scanning sample.

Table 1: Resolution of images with different magnifications.

Magnification	600x	1200x	2000x
Pixel accuracy (μm/pixel)	0.481	0.240	0.145

pressure difference between the two ends of the pipe, which is expressed in MPa; μ is hydrodynamic viscosity, which is expressed in Pa•s; L is the length of the cylindrical pipe, which is expressed in μm; R is the radius of the cylindrical tube, which is expressed in μm. By integrating Equation (2) over the entire cross-section, the total volume flow of the fluid through the cross-section of the pipeline can be obtained as follows:

$$Q = \frac{\pi R^4 \Delta P}{8\mu L}. \tag{3}$$

As seen in Figure 3, it is considered that the total flow through the pore structure of the sample and the total flow through each small pore are equal to each other, then it can be obtained:

$$Q = \sum Q_i, \tag{4}$$

where Q is the total instantaneous flow of the sample microstructure, expressed in mm^3/s; Q_i is the flow rate of each tiny pore expressed in mm^3/s. As seen from Darcy's law, the flow of fluids also follows Darcy's law:

$$Q = \frac{kA}{\mu L}\Delta P, \tag{5}$$

where k is permeability, which is expressed in m^2; A is the cross-sectional area of the fluid, which is expressed in mm^2.

In combination with (3), (4), and (5), the following can be obtained:

$$\frac{kA}{\mu L}\Delta P = Q = \sum Q_i = \sum \frac{\pi R_i^4}{8\mu L}\Delta P. \tag{6}$$

The expression of permeability can be further simplified as follows:

$$k = \frac{\pi}{8A}\sum R_i^4 = \frac{1}{8A}\sum A_i R_i^2, \tag{7}$$

where R_i is pore radius, which is expressed in mm; A_i is the radius R_i of pore area, which is expressed in mm^2.

According to Equation (7) and the simplified internal pore, the permeability of sandstone can be predicted by a digital image.

3. Results and Analysis

3.1. Gray Threshold Selection. As shown in Figure 4, digital images with different magnification are adopted in this study, showing that SEM images can more intuitively observe the pore structure of sandstone. The darker pixels mean the pore of sandstone, while the lighter pixels are seen as the matrix. Before the quantitative characterization of the pore structure, image preprocessing is needed to lay a foundation for subsequent analysis. Brightness and contrast adjustments, image denoising, and image enhancement are all examples of image preprocessing. Generally speaking, for SEM images, the image quality is usually better. Image denoising does not have a significant impact on the subsequent characterization of the image. The change in brightness will not significantly affect the shape of the gray distribution curve (within a specific range). However, the difference in contrast has a significant effect on the shape of the gray distribution curve. Through the above method, the digital image obtained by processing is shown in Figure 5. It can be seen that the pore and matrix structure

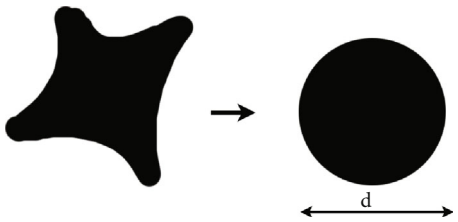

(a) Principle of discrete pore size distribution algorithm

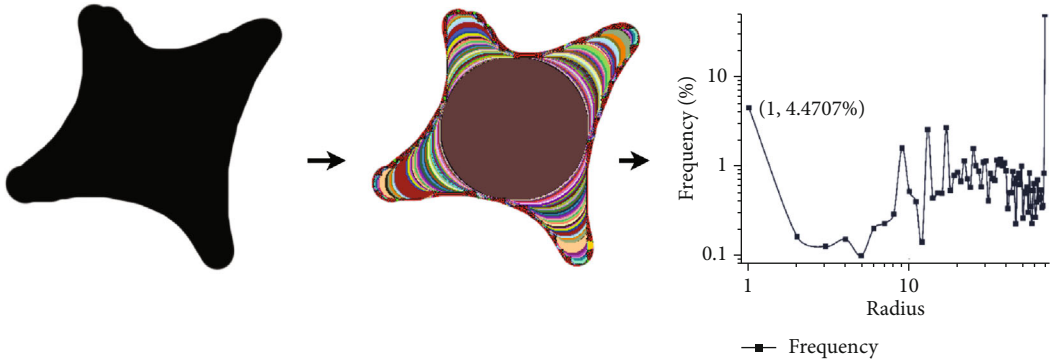

(b) Principle of continuous pore size distribution algorithm

Figure 2: Comparison of calculation principles between DPSD and CPSD with the same pore structure.

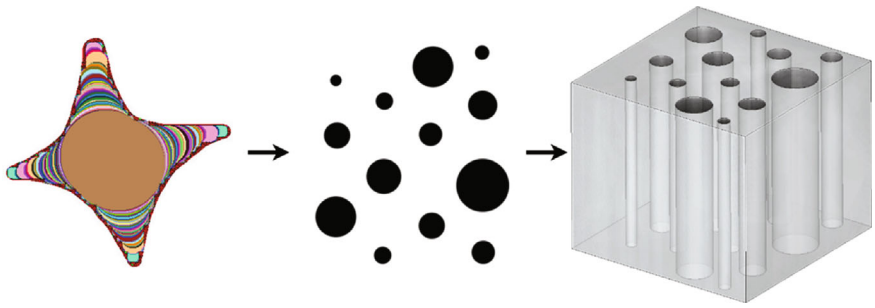

Figure 3: Capillary bundle model of porous media.

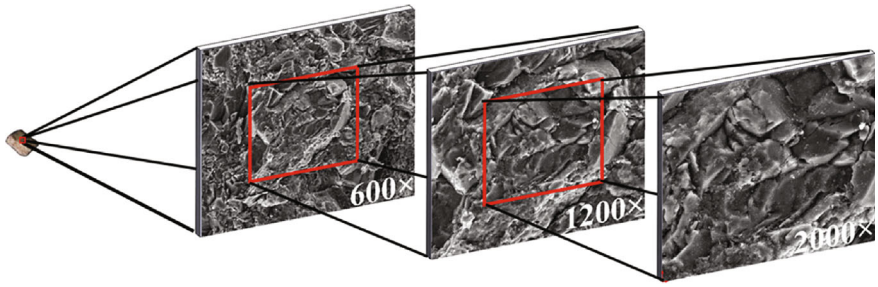

Figure 4: SEM images of different scales of a sandstone sample.

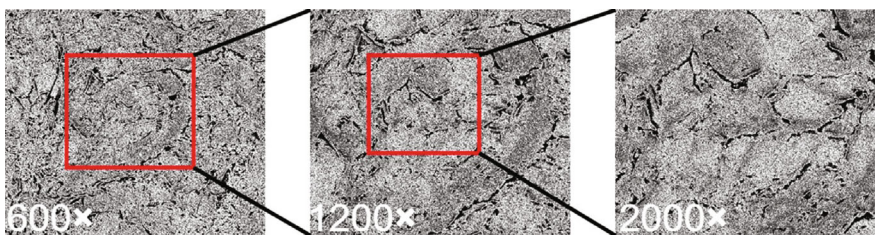

Figure 5: SEM images after preprocessing.

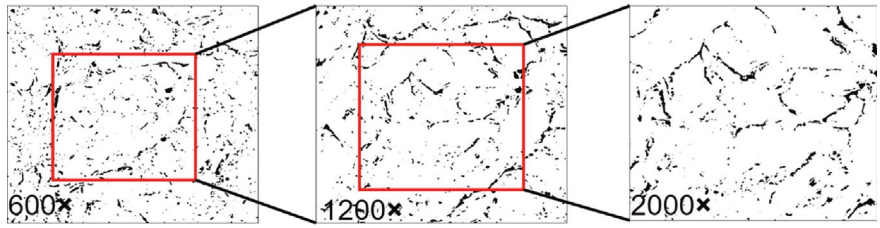

Figure 6: SEM images after segmentation.

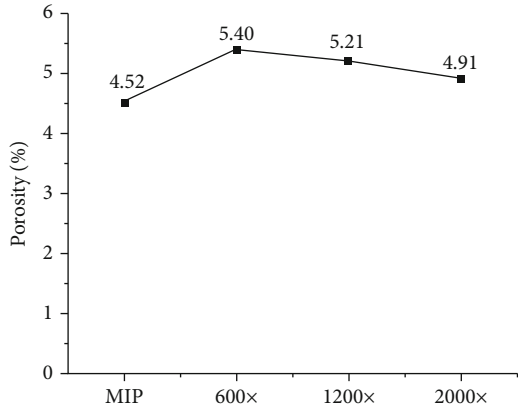

Figure 7: Porosity calculation results based on digital images and MIP.

can be better identified and distinguished in the preprocessed image.

The segmentation threshold is the most important way to segment a pore structure from the digital image. The threshold determination methods suitable for geomaterials are mainly divided into threshold algorithm determination and artificial selection. Different algorithms have a significant impact on threshold determination and subsequent segmentation results. Therefore, a detailed comparative analysis is required to reach a more appropriate threshold value before determining the threshold value. In particular, the thresholds of digital images with different magnifications are 21, 23, and 28, respectively. After binary segmentation [2, 3], the binary image is shown in Figure 6, where we can see that the pore structure can be easily virtually identified.

3.2. Pore Structure Characteristics of Images with Different Scales

3.2.1. Porosity Calculation. According to the threshold segmentation results in the previous section, combined with Equation (1), the porosity of images with different magnifications is shown in Figure 7. Compared with the MIP result, it can be seen that the extraction results of apparent porosity are relatively close to the MIP result, especially when the magnification is 2000 times. According to Figure 7, it can be seen that the porosity extracted from the SEM digital image of sandstone is relatively reliable, although there are some differences.

3.2.2. Pore Size Distribution Calculation. This work determines the distribution of pore sizes in a microscopic image at different magnifications based on CPSD and DPSD techniques mentioned in Munch's research. The pore sizes measured by MIP can be found to be smaller than those based on digital images. The pixel accuracy of the 2000x image is 0.145 μm (continuous) and 0.08 μm (discrete), while the pore size range of the CPSD experiment is 0.004-0.25 μm. The CPSD results are closer to the MIP than the CPSD results. The peak pore size for the three magnification images is 1.44 μm (30.64%), 0.72 μm (27.68%), and 0.43 μm (21.33%), respectively. Thus, most pores that can be characterized based on digital image techniques are on the micron scale. It is interesting to note that digital image-based methods can effectively characterize large pores, whereas MIP completely ignores pores of this scale. Therefore, the pore size distribution can be better represented at full scale if the two tools are combined.

Figures 8(a) and 8(b) show the calculation results based on CPSD and DPSD. Although the two calculation methods are fundamentally different, at 600 magnification, large pores account for a greater proportion of the results. On the contrary, most of the calculation results at a magnification of 2000 are small-sized pores. Apparently, as the magnification increases, the field of view of the image is reduced to a certain extent, and obtained pores are less, so the proportion of pores of different sizes change to a particular time. Comparing the pore size distribution in the same image obtained by various methods, it is found that the large-sized pores account for a more significant proportion of the DPSD calculation results based on the same image. Still, the CPSD calculation results are primarily small- and medium-sized pores. Therefore, the pore size measured by DPSD is too large.

3.3. Permeability Prediction Based on Images with Different Scales.

Based on the pore size distribution obtained in the previous work, we used the Hagen-Poiseuille method to calculate sample's permeability. The calculation results are shown in Figure 9.

The predicted permeability values were found to be decreasing as the magnification increased: the permeability calculated for the three magnification images were 2.49×10^{-14} m^2 (discrete 9.21×10^{-14} m^2), 8.14×10^{-14} m^2 (4.08×10^{-14} m^2), and 3.94×10^{-14} m^2 (2.16×10^{-14} m^2), respectively. According to the principle of permeability calculation, it is clear that the permeability size is closely related to the pore size distribution and porosity. In addition, it can

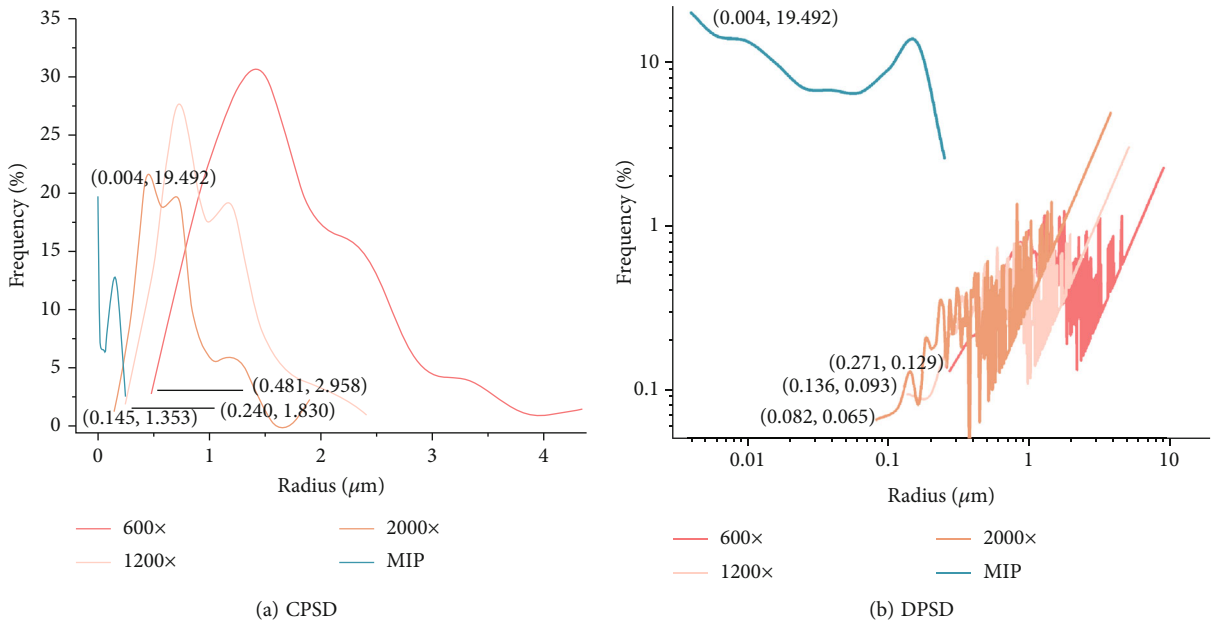

(a) CPSD (b) DPSD

Figure 8: Calculation results of pore size distribution based on digital images and MIP.

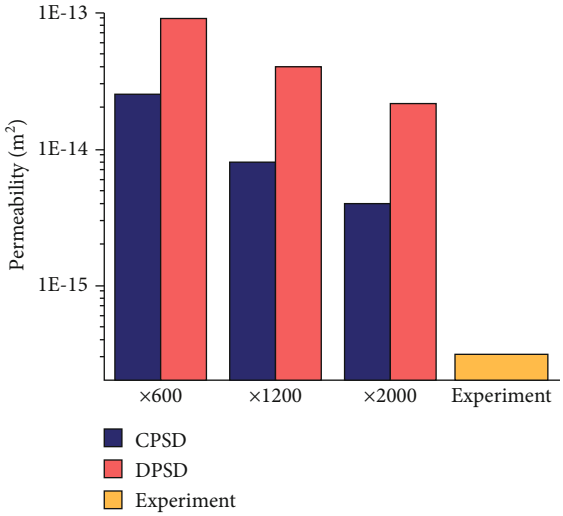

Figure 9: Permeability calculation results based on digital images and laboratory experiments.

be found that the proportion of pore area in the field of view is more significant, and most of them are large pores, with tiny pores below 0.6 μm accounting for only 3%. Hence, its permeability prediction is higher when image's magnification is 600. While the proportion is of 2000 rises to 50%. Meanwhile, according to Figure 7, the figure of porosity shows a marked decrease, and there is a similar trend in the volume of pore space per unit area of view, leading to the drop of permeability.

Compared to DPSD, the value of permeability prediction by CPSD is smaller. Although DPSD measures a slight increase in the proportion of macropores, DPSD classifies and sizes pores based on the connectivity components of the binary image. In contrast, CPSD treats pixels that can be covered in a moving sweep of same-sized circles as same-sized pores. In order to convert the pore size and area obtained by CPSD into the permeability value of the Hagen-Poiseuille formula, we use Equation (7), assuming that the pores are circular. After that, they used the radius of the circle instead of the radius of the corresponding area circle to calculate the pore size. Specifically, as in the first step of Figure 3, the large pore sizes are primarily concentrated in the middle of the port area, where the radius of the equivalent area circle is larger than the radius of the maximum inner tangent circle. However, the CPSD pore size considers the maximum inner tangent circle radius, as detailed by Muench and Holzer [16]. It means that the same pore, compared to the DPSD, is treated by the CPSD as several smaller pore sizes. Therefore, the CPSD measurement leads to a small permeability prediction based on the Hagen-Poiseuille hypothesis about the pore geometry.

The predicted value is higher when compared to the measured value. The difference between the two is 1 to 2 orders of magnitude. Pore spaces of tiny size are difficult to perceive and measure due to image acquisition magnification limitations. In addition, the tortuosity of the pore network is not considered in the permeability calculations, nor is the complexity of the 3D pore network. These result in a large gap between the predicted permeability values based on microscopic images and equipment testing. In the future, the superposition and fusion of some images of different scales can be carried out to obtain an accurate three-dimensional model based on multiscale digital images. Furthermore, some quantitative characterization experiments based on the cross-scale 3D digital model may be closer to the experimental test results.

4. Conclusion

In this paper, a scanning electron microscope is used to obtain images of a sandstone sample for different magnifications of its microstructure. A threshold segmentation method is selected to segment the image. Then, the pore distribution of different sizes is measured based on the continuous pore size distribution and discrete pore size distribution methods. Finally, the Hagen-Poiseuille permeability calculation method is selected based on digital images to calculate sample's permeability.

The magnification of the image acquisition affects the perceived porosity and subsequent calculations. It is found that the magnification of the image has a noticeable effect on the characterization of the pore structure. As the magnification increases, the field of view of the image becomes smaller, and the perceived pores are less. The greater the magnification, the more pores, and medium pores are observed. As the proportion of macropores decreases, the predicted value of permeability decreases slightly. Pore distribution measurement methods have a noticeable impact on the pore size statistics and permeability calculations. Due to the difference in the pore size calculation principle of the two algorithms, the permeability calculated based on CPSD is lower than that of DPSD, which is larger than the experimental result. The difference is about one to two orders of magnitude. In the future, to obtain a more accurate prediction, a three-dimensional digital model should be established. There are usually two ways to get a three-dimensional digital model. One is to perform three-dimensional reconstruction through X-CT scanning. Another method is to use the simulated annealing method to reconstruct the SEM image in three dimensions. Additionally, the tortuosity of the pore network and the complexity of the 3D pore network should be considered.

Data Availability

Some or all data, models, or code generated or used during the study are available from the corresponding author by request.

Conflicts of Interest

The authors declare that they have no conflicts of interest.

Acknowledgments

The authors are grateful for the support of the National Natural Science Foundation of China (nos. 51809263 and 52174133), the Open Fund of MOE Key Laboratory of Deep Earth Science and Engineering, Sichuan University (grant no. DESE201906), and the Fundamental Research Funds for the Central Universities (China University of Mining and Technology) (2019ZDPY13).

References

[1] Y. Chen, S. Hu, K. Wei, R. Hu, C. Zhou, and L. Jing, "Experimental characterization and micromechanical modeling of damage-induced permeability variation in Beishan granite," *International Journal of Rock Mechanics and Mining Sciences*, vol. 71, pp. 64–76, 2014.

[2] J. F. Liu, X.-L. Cao, J. Xu, Q.-L. Yao, and H.-Y. Ni, "A new method for threshold determination of gray image," *Geomechanics and Geophysics for Geo-Energy and Geo-Resources*, vol. 6, no. 4, p. 72, 2020.

[3] J. Liu, S. Song, X. Cao et al., "Determination of full-scale pore size distribution of Gaomiaozi bentonite and its permeability prediction," *Journal of Rock Mechanics and Geotechnical Engineering*, vol. 12, no. 2, pp. 403–413, 2020.

[4] S. Tao, Z. J. Pan, S. D. Chen, and S. Tang, "Coal seam porosity and fracture heterogeneity of marcolithotypes in the Fanzhuang Block, southern Qinshui Basin, China," *Journal of Natural Gas Science and Engineering*, vol. 66, pp. 148–158, 2019.

[5] T. Hagengruber, M. Taha, E. Rougier, E. E. Knight, and J. C. Stormont, "Evolution of permeability in sandstone during confined Brazilian testing," *Rock Mechanics and Rock Engineering*, 2021.

[6] Y.-L. Kang and P.-Y. Luo, "Current status and prospect of key techniques for exploration and production of tight sandstone gas reservoirs in China," *Petroleum Exploration and Development*, vol. 34, no. 2, pp. 239–245, 2007.

[7] J. F. Liu, H. Y. Ni, H. Pu, Q. L. Yao, and X. B. Mao, "Test theory, method and device of gas permeability of porous media and the application," *Chinese Journal of Rock Mechanics and Engineering*, vol. 40, no. 1, pp. 137–146, 2021.

[8] W. M. Ye, Y. J. Cui, L. X. Qian, and B. Chen, "An experimental study of the water transfer through confined compacted GMZ bentonite," *Engineering Geology*, vol. 108, no. 3-4, pp. 169–176, 2009.

[9] T. Meng, X. Yongbing, J. Ma et al., "Evolution of permeability and microscopic pore structure of sandstone and its weakening mechanism under coupled thermo-hydro-mechanical environment subjected to real-time high temperature," *Engineering Geology*, vol. 280, article 105955, 2021.

[10] G. Zou, J. She, S. Peng, Q. Yin, H. Liu, and Y. Che, "Two-dimensional SEM image-based analysis of coal porosity and its pore structure," *International Journal of Coal Science & Technology*, vol. 7, no. 2, pp. 350–361, 2020.

[11] L. M. Anovitz, J. T. Freiburg, M. Wasbrough et al., "The effects of burial diagenesis on multiscale porosity in the St. Peter Sandstone: an imaging, small-angle, and ultra-small-angle neutron scattering analysis," *Marine and Petroleum Geology*, vol. 92, pp. 352–371, 2018.

[12] S. Tao, S. Chen, D. Tang, X. Zhao, H. Xu, and S. Li, "Material composition, pore structure and adsorption capacity of low-rank coals around the first coalification jump: a case of eastern Junggar Basin, China," *Fuel*, vol. 211, pp. 804–815, 2018.

[13] S. B. Song, J. F. Liu, H. Y. Ni, X. L. Cao, H. Pu, and B. X. Huang, "A new automatic thresholding algorithm for unimodal gray-level distribution images by using the gray gradient information," *Journal of Petroleum Science and Engineering*, vol. 190, pp. 107074–107077, 2020.

[14] R. Wirth, "Focused ion beam (FIB) combined with SEM and TEM: advanced analytical tools for studies of chemical composition, microstructure and crystal structure in geomaterials on a nanometre scale," *Chemical Geology*, vol. 261, no. 3-4, pp. 217–229, 2009.

[15] F. Zhang, Z. Jiang, W. Sun et al., "A multiscale comprehensive study on pore structure of tight sandstone reservoir realized by

nuclear magnetic resonance, high pressure mercury injection and constant-rate mercury injection penetration test," *Marine and Petroleum Geology*, vol. 109, pp. 208–222, 2019.

[16] B. Muench and L. Holzer, "Contradicting geometrical concepts in pore size analysis attained with electron microscopy and mercury intrusion," *Journal of the American Ceramic Society*, vol. 91, no. 12, pp. 4059–4067, 2008.

[17] S. P. S. R. Skalak, "The history of Poiseuille's law," *Annual Review of Fluid Mechanics*, vol. 25, no. 1, pp. 1–20, 1993.